Cellular senescence and inflammation in aging and age-related disease

Wijshake, Tobias

CHAPTER 2

Clearance of p16^{Ink4a}-positive senescent cells delays ageing-associated disorders

Darren J. Baker, Tobias Wijshake, Tamar Tchkonia, Nathan K. LeBrasseur, Bennett G. Childs, Bart van de Sluis, James L. Kirkland & Jan M. van Deursen

Nature 479, 232-236 (2011)

LETTER

doi:10.1038/nature10600

Clearance of p16^{Ink4a}-positive senescent cells delays ageing-associated disorders

Darren J. Baker[1,2,3], Tobias Wijshake[1,4], Tamar Tchkonia[3], Nathan K. LeBrasseur[3,5], Bennett G. Childs[1], Bart van de Sluis[4], James L. Kirkland[3] & Jan M. van Deursen[1,2,3]

Advanced age is the main risk factor for most chronic diseases and functional deficits in humans, but the fundamental mechanisms that drive ageing remain largely unknown, impeding the development of interventions that might delay or prevent age-related disorders and maximize healthy lifespan. Cellular senescence, which halts the proliferation of damaged or dysfunctional cells, is an important mechanism to constrain the malignant progression of tumour cells[1,2]. Senescent cells accumulate in various tissues and organs with ageing[3] and have been hypothesized to disrupt tissue structure and function because of the components they secrete[4,5]. However, whether senescent cells are causally implicated in age-related dysfunction and whether their removal is beneficial has remained unknown. To address these fundamental questions, we made use of a biomarker for senescence, p16^{Ink4a}, to design a novel transgene, *INK-ATTAC*, for inducible elimination of p16^{Ink4a}-positive senescent cells upon administration of a drug. Here we show that in the BubR1 progeroid mouse background, *INK-ATTAC* removes p16^{Ink4a}-positive senescent cells upon drug treatment. In tissues—such as adipose tissue, skeletal muscle and eye—in which p16^{Ink4a} contributes to the acquisition of age-related pathologies, life-long removal of p16^{Ink4a}-expressing cells delayed onset of these phenotypes. Furthermore, late-life clearance attenuated progression of already established age-related disorders. These data indicate that cellular senescence is causally implicated in generating age-related phenotypes and that removal of senescent cells can prevent or delay tissue dysfunction and extend healthspan.

To examine the role of cellular senescence in ageing and age-related pathologies, we designed a transgenic strategy for the clearance of senescent cells in mice. We based our approach on an earlier mouse model, termed FAT-ATTAC (fat apoptosis through targeted activation of caspase), in which adipocytes were selectively killed by apoptosis upon the administration of AP20187, a synthetic drug that induces dimerization of a membrane-bound myristoylated FK506-binding-protein–caspase 8 (FKBP–Casp8) fusion protein expressed specifically in adipocytes via the minimal *Fabp4* promoter[6]. Although a universal marker that is solely expressed in senescent cells has not been identified, most senescent cells seem to express p16^{Ink4a}, a cyclin-dependent kinase inhibitor and tumour suppressor that enforces growth arrest by activating Rb[5,7]. Additionally, the expression of p16^{Ink4a} is known to increase with ageing in several rodent and human tissues[8]. We replaced the *Fabp4* promoter with a 2,617-bp fragment of the *p16*^{Ink4a} gene promoter that is transcriptionally active in senescent, but not non-senescent cells (Fig. 1a)[9]. We added an internal ribosome entry site (IRES) followed by an open reading frame (ORF) coding for enhanced green fluorescence protein (EGFP) to allow for detection and collection of p16^{Ink4a}-positive senescent cells. Injection of the resulting construct into fertilized eggs yielded nine transgenic *INK-ATTAC* founder lines.

To examine whether removal of p16^{Ink4a}-expressing cells is technically feasible and whether this affects age-associated deficits in mice, we bred each of the founder lines onto a *BubR1* hypomorphic (*BubR1*$^{H/H}$) genetic background. *BubR1* encodes a key member of the mitotic checkpoint, a surveillance mechanism that ensures accurate chromosome segregation in mitosis by inhibiting the ubiquitin ligase activity of Cdc20-activated anaphase-promoting complex (APC^{Cdc20}) in the presence of unattached chromosomes[10,11]. *BubR1*$^{H/H}$ mice have a markedly shortened lifespan and exhibit a variety of age-related phenotypes, including infertility, lordokyphosis, sarcopenia, cataracts, fat loss, cardiac arrhythmias, arterial wall stiffening, impaired wound healing and dermal thinning[12–14]. It has been proposed that BubR1 is a determinant of natural ageing, because levels of BubR1 decline markedly with age[12–14]. *BubR1*$^{H/H}$ mice selectively accumulate p16^{Ink4a}-positive cells in certain tissues in which age-associated pathologies develop, including adipose tissue, skeletal muscle and eye[15]. Inactivation of *p16*^{Ink4a} in these mice is known to delay the onset of age-related phenotypes selectively in these tissues[15]. To screen for *INK-ATTAC* transgene activity in p16^{Ink4a}-positive cells, we collected samples of inguinal adipose tissue (IAT) from each of the nine *BubR1*$^{H/H}$;*INK-ATTAC* strains at 5 months of age and analysed them for GFP expression by fluorescence microscopy. We observed GFP fluorescence in two of these strains, *BubR1*$^{H/H}$;*INK-ATTAC-3* and *-5* (Fig. 1b and Supplementary Fig. 1a). Quantitative reverse transcription–polymerase chain reaction (qRT–PCR) analysis of various tissues from *BubR1*$^{H/H}$;*INK-ATTAC-3* and *-5* mice demonstrated that *INK-ATTAC* and *GFP* transcript levels were significantly elevated in adipose tissue, skeletal muscle and eye, but not in tissues in which endogenous p16^{Ink4a} is not induced, including liver and heart (Fig. 1c and Supplementary Fig. 1b).

To confirm that transgenic *INK-ATTAC* and endogenous *p16*^{Ink4a} are under the same transcriptional control mechanism outside the context of BubR1 hypomorphism, we harvested bone marrow cells from 2-month-old wild-type (*WT*);*INK-ATTAC-3* and *-5* mice and cultured them in the absence or presence of rosiglitazone, a drug that can induce cellular senescence and *p16*^{Ink4a} expression through activation of PPARγ[16]. Immunofluorescence microscopy revealed that a high proportion of cells expressed Flag-tagged FKBP–Casp8 in the presence of rosiglitazone, but not in its absence (Fig. 1d). Furthermore, we observed selective *INK-ATTAC* transgene induction in tissues of *WT*;*INK-ATTAC-3* mice showing elevated expression of endogenous *p16*^{Ink4a} upon chronological ageing (Supplementary Fig. 2). Together, these data indicate that *INK-ATTAC* gene activity in founder lines 3 and 5 overlaps with endogenous *p16*^{Ink4a} expression.

Next, we tested whether *INK-ATTAC* is expressed in senescent cells in BubR1 hypomorphic tissue. Fat tissue of aged *BubR1*$^{H/H}$;*INK-ATTAC* mice stained strongly for senescence-associated-β-galactosidase (SA-β-Gal; Fig. 1e). qRT–PCR analysis demonstrated that *INK-ATTAC* expression correlates with expression of senescence markers in IAT (Fig. 1f and Supplementary Fig. 3a). Skeletal muscle and lens tissue of aged *BubR1*$^{H/H}$;*INK-ATTAC* mice are SA-β-Gal negative (data not shown), but both these tissues expressed other markers of senescence

[1]Department of Pediatric and Adolescent Medicine, Mayo Clinic College of Medicine, Rochester, Minnesota 55905, USA. [2]Molecular Biology and Biochemistry, Mayo Clinic College of Medicine, Rochester, Minnesota 55905, USA. [3]Robert and Arlene Kogod Center on Aging, Mayo Clinic College of Medicine, Rochester, Minnesota 55905, USA. [4]Department of Pathology and Medical Biology, University Medical Center Groningen, Groningen University, Groningen 9700 RB, The Netherlands. [5]Physical Medicine and Rehabilitation, Mayo Clinic College of Medicine, Rochester, Minnesota 55905, USA.

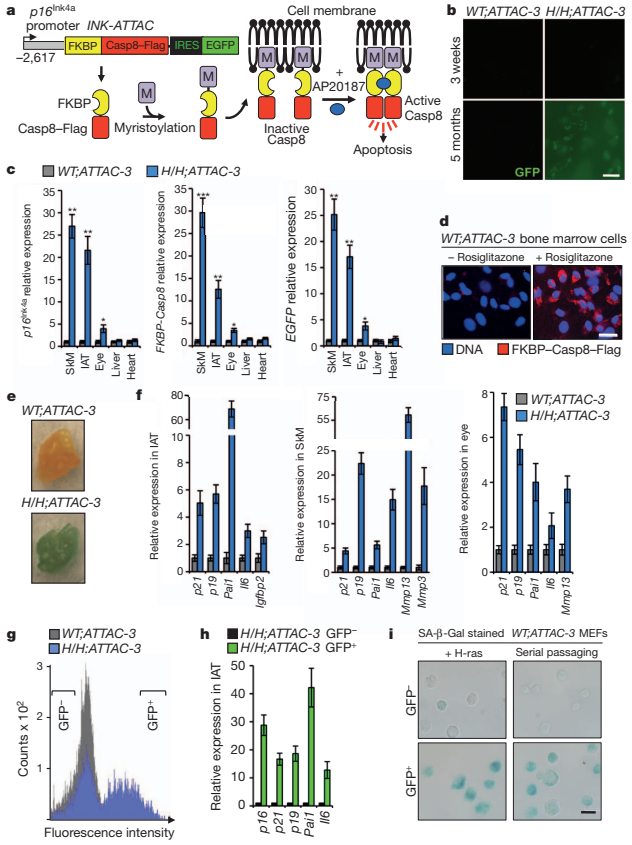

Figure 1 | Generation and characterization of *INK-ATTAC* transgenic mice. **a**, Schematic of the *INK-ATTAC* construct and the mechanism of apoptosis activation. **b**, GFP intensity of IAT. **c**, qRT–PCR analysis of the indicated tissues of 10-month-old mice. *ATTAC, INK-ATTAC*; *H/H, BubR1*$^{H/H}$; SkM, skeletal muscle (gastrocnemius). **d**, Bone marrow cells harvested from 2-month-old mice immunostained for Flag after culture in the absence or presence of rosiglitazone for 48 h. **e**, SA-β-Gal stained IAT collected from 9-month-old mice of the indicated genotypes. **f**, Expression of senescence markers in tissues of 10-month-old mice measured by qRT–PCR. All increases are statistically significant ($P < 0.05$). **g**, FACS profile of single-cell suspensions from IAT of 10-month-old mice. Brackets indicate sorting gates. **h**, GFP$^+$ and GFP$^-$ cell populations from IAT analysed for relative expression of senescence markers by qRT–PCR. All increases are statistically significant ($P < 0.01$). **i**, Bright field images of MEFs sorted into GFP$^+$ and GFP$^-$ populations after induction of senescence and then stained for SA-β-Gal. For all experiments, $n = 3$ untreated females per genotype. Error bars, s.d. Scale bars in **b**, **d** and **i**, 20 μm. $^*P < 0.05$, $^{**}P < 0.01$, $^{***}P < 0.001$.

(Fig. 1f and Supplementary Fig. 3a). Senescence markers were not elevated in 3-week-old *BubR1*$^{H/H}$;*INK-ATTAC* mice (Supplementary Fig. 3b, c). To obtain additional evidence for selective expression of *INK-ATTAC* in senescent cells, we collected IAT from aged *BubR1*$^{H/H}$;*INK-ATTAC* animals, prepared single-cell suspensions by collagenase treatment, separated GFP$^+$ and GFP$^-$ cell populations by fluorescence activated cell sorting (FACS; Fig. 1g), and analysed each population for expression of *INK-ATTAC* and senescence markers by qRT–PCR. GFP$^+$ cells not only expressed much higher levels of *p16*^{Ink4a} than GFP$^-$ cells but also had elevated levels of other key senescence markers (Fig. 1h and Supplementary Fig. 3d). Furthermore, two conditions that induce p16^{Ink4a} expression and senescence in primary mouse embryonic fibroblasts (MEFs), ectopic expression of oncogenic Ras and serial passaging[12,17,18], produced a subpopulation of GFP$^+$ *WT;INK-ATTAC-3* MEFs that, in contrast to the remaining GFP$^-$ cells, stained positively for SA-β-Gal (Fig. 1i). Taken together, these results indicate that *INK-ATTAC* is selectively expressed in p16^{Ink4a}-positive senescent cells.

To determine whether *INK-ATTAC* can eliminate senescent cells, we cultured bone marrow cells of *WT;INK-ATTAC* transgenic lines 3 and 5 in the presence of rosiglitazone to induce senescence and then monitored cell survival after activating the FKBP–Casp8 fusion protein by AP20187 treatment. We found that the vast majority of cells from both transgenic lines were either dead or in the process of dying 48 h after adding AP20187 (Fig. 2a). In contrast, parallel cultures that remained untreated consisted almost entirely of viable SA-β-Gal-positive cells. These data show that FKBP–Casp8 activation efficiently eliminates p16^{Ink4a}-positive senescent cells *in vitro*.

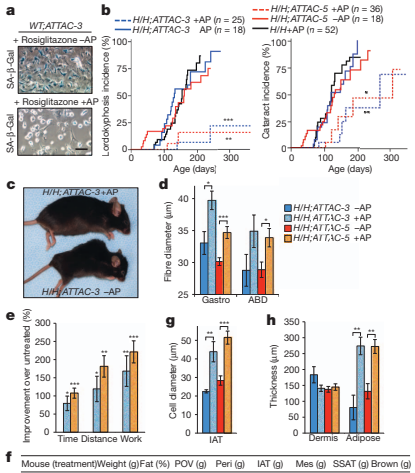

f

Mouse (treatment)	Weight (g)	Fat (%)	POV (g)	Peri (g)	IAT (g)	Mes (g)	SSAT (g)	Brown (g)
H/H;ATTAC-3 (–AP)	17.4 (1.8)	15.6 (3.4)	0.054 (0.05)	0.016 (0.02)	0.058 (0.02)	0.063 (0.05)	0.038 (0.01)	0.084 (0.005)
H/H;ATTAC-3 (+AP)	21.3* (3.8)	28.6*** (4.1)	0.334* (0.28)	0.069 (0.06)	0.192* (0.12)	0.151 (0.09)	0.095** (0.03)	0.119 (0.053)
H/H;ATTAC-5 (–AP)	16.7 (2.2)	15.4 (2.5)	0.137 (0.13)	0.020 (0.01)	0.075 (0.05)	0.061 (0.04)	0.050 (0.02)	0.104 (0.030)
H/H;ATTAC-5 (+AP)	24.0*** (2.1)	27.4*** (4.2)	0.433** (0.11)	0.071** (0.02)	0.225** (0.10)	0.262* (0.17)	0.115* (0.06)	0.159** (0.029)

Figure 2 | *BubR1*$^{H/H}$*;INK-ATTAC* mice treated with AP20187 from weaning age on show delayed onset of p16^{Ink4a}-mediated age-related phenotypes. **a**, Bone marrow cells cultured in rosiglitazone for 5 days and then treated or not treated with AP20187 (AP) for 2 days before SA-β-Gal staining. Scale bar, 50 μm. **b**, Incidence of lordokyphosis and cataracts. **c**, Representative images of 9-month-old mice. **d**, Mean skeletal muscle fibre diameters of 10-month-old mice. ABD, abdominal muscle; Gastro, gastrocnemius muscle. **e**, Exercise ability of 10-month-old AP20187-treated mice relative to age-matched untreated mice. Time is running time to exhaustion; distance is distance travelled at time of exhaustion; work is the energy expended to exhaustion. **f**, Body and fat depot weights of 10-month-old mice. Parentheses, s.d. Mes, mesenteric; Peri, perirenal; POV, paraovarian; SSAT, subscapular adipose tissue. **g**, Average fat cell diameters in IAT of 10-month-old mice. **h**, Dermis and subdermal adipose layer thickness of 10-month-old mice. Colour codes in **e**, **g** and **h** are as indicated in **d**. Error bars, s.e.m. For all analysis $n = 6$ female mice per genotype (per treatment). $^{*}P < 0.05$, $^{**}P < 0.01$, $^{***}P < 0.001$.

Next, we examined whether clearance of p16^{Ink4a}-expressing cells from *BubR1*$^{H/H}$ mice prevents or delays the onset of age-related phenotypes in this progeroid background. To this end, we established cohorts of *BubR1*$^{H/H}$*;INK-ATTAC-3* and *-5* mice, which were either treated with AP20187 every third day beginning at 3 weeks of age or left untreated. Both treated and untreated mice were monitored for the development of age-associated deficits known to accompany p16^{Ink4a} induction, including sarcopenia, cataracts and loss of adipose tissue[15]. Remarkably, treated mice of both *BubR1*$^{H/H}$*;INK-ATTAC* lines had substantially delayed onset of lordokyphosis (a measure of sarcopenia onset in this model[15]) and cataracts compared to untreated mice (Fig. 2b, c). Consistent with decreased lordokyphosis, muscle fibre diameters of AP20187-treated *BubR1*$^{H/H}$*;INK-ATTAC* animals were larger than those of untreated counterparts (Fig. 2d). In addition to muscle retention, treadmill exercise tests revealed that duration of exercise, distance travelled and overall amount of work performed were all significantly increased in the animals treated with AP20187 (Fig. 2e), indicating preservation of muscle function. Dual-energy X-ray absorptiometry (DEXA) scans of *BubR1*$^{H/H}$*;INK-ATTAC* mice confirmed that AP20187 treatment prevented loss of adipose tissue (Fig. 2f). All major fat deposits were larger in AP20187-treated *BubR1*$^{H/H}$*;INK-ATTAC* animals (Fig. 2f) and individual adipocytes were markedly increased in size (Fig. 2g). Consistent with this generally increased adiposity, lateral skin contained significantly more subdermal adipose tissue (Fig. 2h). The above age-related phenotypes were not delayed upon AP20187 treatment of *BubR1*$^{H/H}$ mice lacking *INK-ATTAC* (Fig. 2b and Supplementary Fig. 4).

Age-related phenotypes of *BubR1*$^{H/H}$ mice that arise in a p16^{Ink4a}-independent fashion, such as cardiac arrhythmias and arterial wall stiffening[14], were not attenuated in AP20187-treated *BubR1*$^{H/H}$*;INK-ATTAC* mice (Supplementary Fig. 5a, b). This correlated with lack of *INK-ATTAC* induction in heart and aorta (Fig. 1c and Supplementary Fig. 5c). Cardiac failure is presumably the main cause of death in *BubR1*$^{H/H}$ mice (data not shown), which could explain why the overall survival of AP20187-treated *BubR1*$^{H/H}$*;INK-ATTAC* mice was not substantially extended (Supplementary Fig. 5d). To examine whether clearance of p16^{Ink4a}-positive cells might have any overtly negative side effects, *WT;INK-ATTAC* mice were continuously treated with AP20187 until 8 months of age; however, no such effects were observed (data not shown). Taken together, these results indicate that continuous removal of p16^{Ink4a}-expressing cells from *BubR1*$^{H/H}$*;INK-ATTAC*

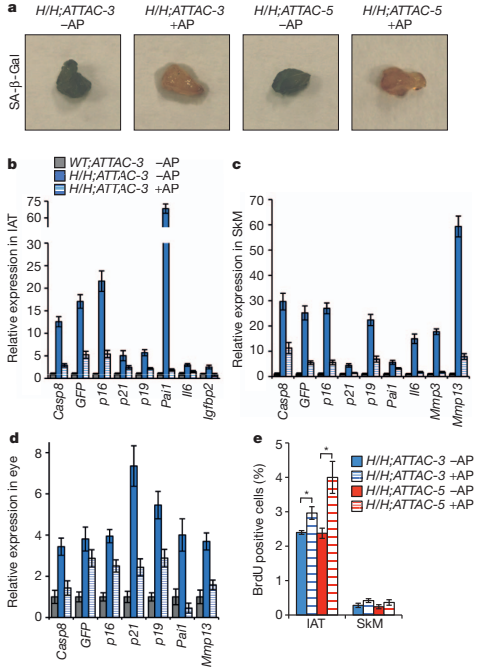

Figure 3 | AP20187-treated *BubR1*$^{H/H}$*;INK-ATTAC* mice have reduced numbers of p16^{Ink4a}-positive senescent cells. **a**, Images of SA-β-Gal stained IAT of 10-month-old mice. **b**–**d**, Expression of senescence markers in IAT (**b**), gastrocnemius (**c**) and eye (**d**) of 10-month-old AP20187-treated and untreated *BubR1*$^{H/H}$*;INK-ATTAC-3* mice relative to age-matched untreated *WT;INK-ATTAC-3* mice. Error bars indicate s.d.; $n = 3$ females per genotype per treatment. The expression of all genes is significantly decreased upon AP20187 treatment ($P < 0.05$) with the exception of *GFP* in the eye. **e**, BrdU incorporation rates in IAT and skeletal muscle. Error bars, s.e.m.; $n = 6$ females per genotype per treatment. $^{*}P < 0.05$.

mice selectively delays age-related phenotypes that depend on $p16^{Ink4a}$ induction.

Next, we determined whether the delayed onset of age-related pathologies coincided with a reduction in the number of senescent cells in these tissues. The IAT of AP20187-treated *BubR1*$^{H/H}$;*INK-ATTAC* mice showed a marked decrease in SA-β-Gal staining compared with the IAT of untreated counterparts (Fig. 3a). Corresponding decreases in other senescence-associated markers were also observed, as well as expected reductions in *INK-ATTAC* and *GFP* (Fig. 3b and Supplementary Fig. 6a). Skeletal muscle and eye had a similar reduction in senescence indicators (Fig. 3c, d and Supplementary Fig. 6b, c). BrdU incorporation was lower in IAT and muscle tissue of untreated than treated animals (Fig. 3e), supporting the contention that senescence-associated replicative arrest is decreased upon administration of AP20187 in *BubR1*$^{H/H}$;*INK-ATTAC* transgenic animals. Together, these data indicate that senescent cells were cleared from tissues and that this delays acquisition of age-related dysfunction in BubR1 hypomorphic mice.

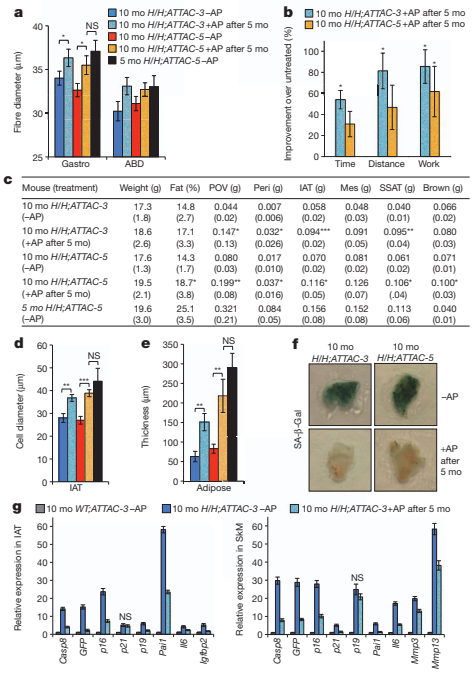

Figure 4 | Treatment of older *BubR1*$^{H/H}$;*INK-ATTAC* mice with AP20187 delays progression of $p16^{Ink4a}$-mediated age-related phenotypes. **a**, Mean skeletal muscle fibre diameters of the indicated mice. ABD, abdominal muscle; Gastro, gastrocnemius muscle. mo, months. **b**, Improvement of exercise ability of the indicated mice relative to age-matched untreated mice. **c**, Body and fat depots weights of the indicated mice. Parentheses, s.d. Mes, mesenteric; Peri, perirenal; POV, paraovarian; SSAT, subscapular adipose tissue. **d**, Average size of fat cells in IAT of the indicated mice. **e**, Subcutaneous adipose layer thickness of the indicated mice. **f**, SA-β-Gal-stained IAT. **g**, Expression of senescence markers in IAT and gastrocnemius of the indicated mice ($n = 3$ females per genotype per treatment). Expression of all genes, except those marked with NS, is significantly decreased ($P < 0.05$) upon late-life AP20187 treatment. Colour codes in **d** and **e** are as indicated in **a**. Error bars indicate s.e.m. except in **g** where they indicate s.d. For analyses in **a**–**f**: $n = 5$ 5-month-old *BubR1*$^{H/H}$;*INK-ATTAC-5* –AP females; $n = 9$ 10-month-old *BubR1*$^{H/H}$;*INK-ATTAC-3* +AP and –AP females; $n = 7$ 10-month-old *BubR1*$^{H/H}$;*INK-ATTAC-5* +AP females; and $n = 8$ 10-month-old *BubR1*$^{H/H}$;*INK-ATTAC-5* –AP females. $^*P < 0.05$, $^{**}P < 0.01$, $^{***}P < 0.001$. NS, not significant.

To investigate the effect of senescent cell clearance later in life when age-related phenotypes are apparent in *BubR1*$^{H/H}$ mice, we started AP20187 treatment of *BubR1*$^{H/H}$;*INK-ATTAC* mice at 5 months instead of weaning age and measured $p16^{Ink4a}$-dependent age-related phenotypes at 10 months. Cataracts had already fully maturated by the onset of AP20187 treatment and remained unchanged (data not shown). Importantly, late-life treated animals had increased mean muscle fibre diameters and showed improved performance in treadmill exercise tests (Fig. 4a, b). Furthermore, most fat depots of these animals were enlarged and adipocyte cell size and subdermal adipose layer thickness were significantly increased (Fig. 4c–e). Senescence markers were substantially reduced in both fat and skeletal muscle of AP20187-treated animals (Fig. 4f, g and Supplementary Fig. 7). Analysis of 5-month-old untreated *BubR1*$^{H/H}$;*INK-ATTAC-5* mice revealed that the observed improvements in skeletal muscle and fat of late-life treated 10-month-old *BubR1*$^{H/H}$;*INK-ATTAC-5* mice reflect attenuated progression of age-related declines rather than a reversal of ageing (Fig. 4a, c–e). Thus, late-life clearance of $p16^{Ink4a}$-positive senescent cells attenuates progression of age-related decline in BubR1 hypomorphic mice.

Whether and how cellular senescence is related to age-related diseases, frailty and dysfunction has been one of the major open questions in the biology of ageing and clinical geriatrics[1]. Here we present a novel transgenic mouse model that allows for the inducible removal of $p16^{Ink4a}$-positive senescent cells. Remarkably, even though transcriptional regulation of endogenous *p16*^{Ink4a} expression is highly complex, involving various transcriptional activators/repressors, epigenetic mechanisms and antisense non-coding RNA[19–22], we find that expression of *INK-ATTAC* driven by a relatively small portion of the *p16*^{Ink4a} promoter closely overlaps with that of endogenous *p16*^{Ink4a}. By breeding *INK-ATTAC* mice into a progeroid mouse genetic background, we show that both life-long and late-life clearance of the $p16^{Ink4a}$-expressing senescent cells selectively delayed age-related pathologies in tissues that accumulate these cells. Furthermore, our data indicate that acquisition of the senescence-associated secretory phenotype (SASP), which enables cells to secrete a variety of growth factors, cytokines and proteases[4], contributes to age-related tissue dysfunction. There were no overt side effects of senescent cell clearance in our model, even though it has been postulated that senescent cells enhance certain types of tissue repair[23,24]. Our proof-of-principle experiments demonstrate that therapeutic interventions to clear senescent cells or block their effects may represent an avenue for treating or delaying age-related diseases and improving healthy human lifespan.

METHODS SUMMARY

Mouse strains and drug treatments. The *INK-ATTAC* transgenic construct was made as follows. The FKBP–Casp8 fragment was subcloned from the aP2-ATTAC transgenic construct[6] (a gift from P. Scherer) and inserted into pBlueScriptII (Stratagene). A 2,617-bp segment of the murine *p16*^{Ink4a} promoter was PCR amplified from BAC DNA to replace the aP2 promoter. An IRES-EGFP fragment was inserted 3′ of the ATTAC. Transgenic founders were obtained by pronuclear injection of the *INK-ATTAC* construct into FVB oocytes. A PCR-based method was used for *INK-ATTAC* transgene identification (primer sequences are available upon request). *BubR1*$^{H/H}$ mice were generated as previously described[12]. For AP20187 (ARIAD Pharmaceuticals) treatments, animals were injected intraperitoneally (i.p.) every 3 days with 0.2 μg g^{-1} body weight of the dimer-inducing drug[6] from weaning ('life-long') or 5-months on ('late-life'). All mice were on a mixed 129 × C57BL/6 × FVB genetic background. Animals were housed in a pathogen-free barrier environment throughout the study. The Institutional Animal Care and Use Committee approved experimental procedures on mice.

Full Methods and any associated references are available in the online version of the paper at www.nature.com/nature.

Received 8 May; accepted 30 September 2011.
Published online 2 November 2011.

1. Campisi, J. Cellular senescence: putting the paradoxes in perspective. *Curr. Opin. Genet. Dev.* **21,** 107–112 (2011).
2. Kuilman, T., Michaloglou, C., Mooi, W. J. & Peeper, D. S. The essence of senescence. *Genes Dev.* **24,** 2463–2479 (2010).
3. Campisi, J. Senescent cells, tumor suppression, and organismal aging: good citizens, bad neighbors. *Cell* **120,** 513–522 (2005).
4. Coppé, J. P. *et al.* Senescence-associated secretory phenotypes reveal cell-nonautonomous functions of oncogenic RAS and the p53 tumor suppressor. *PLoS Biol.* **6,** e301 (2008).
5. Rodier, F. & Campisi, J. Four faces of cellular senescence. *J. Cell Biol.* **192,** 547–556 (2011).
6. Pajvani, U. B. *et al.* Fat apoptosis through targeted activation of caspase 8: a new mouse model of inducible and reversible lipoatrophy. *Nature Med.* **11,** 797–803 (2005).
7. Kim, W. Y. & Sharpless, N. E. The regulation of *INK4/ARF* in cancer and aging. *Cell* **127,** 265–275 (2006).
8. Krishnamurthy, J. *et al. Ink4a/Arf* expression is a biomarker of aging. *J. Clin. Invest.* **114,** 1299–1307 (2004).
9. Wang, W., Wu, J., Zhang, Z. & Tong, T. Characterization of regulatory elements on the promoter region of $p16^{INK4a}$ that contribute to overexpression of p16 in senescent fibroblasts. *J. Biol. Chem.* **276,** 48655–48661 (2001).
10. Malureanu, L. A. *et al.* BubR1 N terminus acts as a soluble inhibitor of cyclin B degradation by APC/C^{Cdc20} in interphase. *Dev. Cell* **16,** 118–131 (2009).
11. Kulukian, A., Han, J. S. & Cleveland, D. W. Unattached kinetochores catalyze production of an anaphase inhibitor that requires a Mad2 template to prime Cdc20 for BubR1 binding. *Dev. Cell* **16,** 105–117 (2009).
12. Baker, D. J. *et al.* BubR1 insufficiency causes early onset of aging-associated phenotypes and infertility in mice. *Nature Genet.* **36,** 744–749 (2004).
13. Hartman, T. K., Wengenack, T. M., Poduslo, J. F. & van Deursen, J. M. Mutant mice with small amounts of BubR1 display accelerated age-related gliosis. *Neurobiol. Aging* **28,** 921–927 (2007).
14. Matsumoto, T. *et al.* Aging-associated vascular phenotype in mutant mice with low levels of BubR1. *Stroke* **38,** 1050–1056 (2007).
15. Baker, D. J. *et al.* Opposing roles for $p16^{Ink4a}$ and $p19^{Arf}$ in senescence and ageing caused by BubR1 insufficiency. *Nature Cell Biol.* **10,** 825–836 (2008).
16. Gan, Q. *et al.* PPARγ accelerates cellular senescence by inducing $p16^{INK4a}$ expression in human diploid fibroblasts. *J. Cell Sci.* **121,** 2235–2245 (2008).
17. Serrano, M., Lin, A. W., McCurrach, M. E., Beach, D. & Lowe, S. W. Oncogenic ras provokes premature cell senescence associated with accumulation of p53 and $p16^{INK4a}$. *Cell* **88,** 593–602 (1997).
18. Kim, H. *et al.* Expression profiles of p53-, $p16^{INK4a}$-, and telomere-regulating genes in replicative senescent primary human, mouse, and chicken fibroblast cells. *Exp. Cell Res.* **272,** 199–208 (2002).
19. Popov, N. & Gil, J. Epigenetic regulation of the *INK4b–ARF–INK4a* locus: in sickness and in health. *Epigenetics* **5,** 685–690 (2010).
20. Gil, J. & Peters, G. Regulation of the *INK4b–ARF–INK4a* tumour suppressor locus: all for one or one for all. *Nature Rev. Mol. Cell Biol.* **7,** 667–677 (2006).
21. Burd, C. E. *et al.* Expression of linear and novel circular forms of an *INK4/ARF*-associated non-coding RNA correlates with atherosclerosis risk. *PLoS Genet.* **6,** e1001233 (2010).
22. Li, J., Poi, M. J. & Tsai, M. D. Regulatory mechanisms of tumor suppressor $P16^{INK4A}$ and their relevance to cancer. *Biochemistry* **50,** 5566–5582 (2011).
23. Krizhanovsky, V. *et al.* Senescence of activated stellate cells limits liver fibrosis. *Cell* **134,** 657–667 (2008).
24. Jun, J. I. & Lau, L. F. The matricellular protein CCN1 induces fibroblast senescence and restricts fibrosis in cutaneous wound healing. *Nature Cell Biol.* **12,** 676–685 (2010).

Supplementary Information is linked to the online version of the paper at www.nature.com/nature.

Acknowledgements We thank W. Zhou, D. Norris, T. Mann, U. Moedder, T. Pirtskhalava and S. Yamada for assistance; S. Khosla, T. von Zglinicki, L. Malureanu, R. Ricke and P. Galardy, and members of the J.M.v.D. laboratory for helpful discussions; and P. Scherer for the gift of the aP2-ATTAC plasmid. This work was supported by the Ellison Medical Foundation (J.M.v.D.), the Noaber Foundation (J.M.v.D. and J.L.K.), the Robert and Arlene Kogod Center on Aging, and the National Institutes of Health (CA96985, J.M.v.D. and AG13925, J.L.K.).

Author Contributions D.J.B., T.T., J.L.K., and J.M.v.D designed the *INK-ATTAC* strategy. D.J.B. and T.W. performed most of the experiments, T.T. did the rosiglitazone experiments, N.K.L. and B.G.C. assisted with the analysis of muscle functionality and *in vitro* senescence, respectively, and B.v.d.S. helped supervise T.W. The manuscript was written by D.J.B. and J.M.v.D. All authors discussed results, made figures and edited the manuscript. J.M.v.D. directed and supervised all aspects of the study.

Author Information Reprints and permissions information is available at www.nature.com/reprints. The authors declare no competing financial interests. Readers are welcome to comment on the online version of this article at www.nature.com/nature. Correspondence and requests for materials should be addressed to J.M.v.D. (vandeursen.jan@mayo.edu).

METHODS

Mouse strains and drug treatments. The *INK-ATTAC* transgenic construct was made as follows. The FKBP–Casp8 fragment was subcloned from the aP2-ATTAC transgenic construct[6] (a gift from P. Scherer) and inserted into pBlueScriptII (Stratagene). A 2,617-bp segment of the murine $p16^{Ink4a}$ promoter was PCR amplified from BAC DNA to replace the aP2 promoter. An IRES-EGFP fragment was inserted 3′ of the ATTAC. Transgenic founders were obtained by pronuclear injection of the *INK-ATTAC* construct into FVB oocytes. A PCR-based method was used for *INK-ATTAC* transgene identification (primer sequences are available upon request). $BubR1^{H/H}$ mice were generated as previously described[12]. For AP20187 (ARIAD Pharmaceuticals) treatments, animals were injected intraperitoneally (i.p.) every 3 days with 0.2 μg g^{-1} body weight of the dimer-inducing drug[6] from weaning ('life-long') or 5-months on ('late-life'). All mice were on a mixed 129 × C57BL/6 × FVB genetic background. Animals were housed in a pathogen-free barrier environment throughout the study. The Institutional Animal Care and Use Committee approved experimental procedures on mice.

Statistical analysis. Prism software was used for the generation of all survival curves and statistical analyses. Two-tailed unpaired *t* tests were used for pairwise significance analysis in the following figures: Fig. 1c, f and h; Fig. 2d–h; Fig. 3b–e; Fig. 4a–e, g; Supplementary Fig. 1b; Supplementary Fig. 2; Supplementary Fig. 3; Supplementary Fig. 4; Supplementary Fig. 5a–c; Supplementary Fig. 6; and Supplementary Fig. 7. Log-rank tests were used to determine overall and pairwise significance for incidence curves in Fig. 2b and survival curves in Supplementary Fig. 5d. For consistency in these comparisons, the following identifies the significance values: $*P < 0.05$, $**P < 0.01$, $***P < 0.001$.

Cell culture. Culture of bone marrow cells was as previously described[25]. Briefly, tibia and femur bones of 2-month-old *WT;INK-ATTAC* transgenic mouse lines were collected and flushed with DMEM containing 15% FBS. After centrifugation at 400*g* for 10 min and counting of viable cells with trypan blue, cells were resuspended in DMEM containing 15% FBS to a final concentration of 5×10^6 viable cells per ml. Initially, cells were plated in 6-well tissue culture dishes at 3.5 ml $well^{-1}$ (1.9×10^6 cells cm^{-2}). Cultures were kept in a humidified 5% CO_2 incubator at 37 °C for 72 h, when non-adherent cells were removed by changing the medium. Assays were performed on cells that had been trypsinized and seeded to confluency in 24-well plates. To induce senescence and evaluate expression of the *INK-ATTAC* transgene, cells were treated with 1 μM rosiglitazone (Cayman Chemical Company) or with vehicle. The accumulation of GFP^+ cells was observed by fluorescence microscopy and transgene expression was verified by immunofluorescence staining for Flag (Origene) as described[26]. After 5 days of rosiglitazone treatment, cells were washed with PBS and treated with vehicle, 1 μM rosiglitazone, 10 nM AP20187, or both. After 48 h, cultures were fixed and stained for SA-β-Gal activity as described[27]. *WT;INK-ATTAC* MEFs were generated and cultured as previously described[12]. For induction of replicative senescence, *WT;INK-ATTAC* MEF cultures were maintained in 20% O_2 for 12–15 passages. For oncogene-induced senescence, early passage MEFs were infected with concentrated pBABE puro H-ras^{G12V} retrovirus (Addgene plasmid 9051) for 48 h. MEFs were then cultured in DMEM containing puromycin (2 μg ml^{-1}) for 5 days. Cells from serial passage and H-ras induced senescence were sorted into GFP^+ and GFP^- populations using a FACS Aria Cell Sorter (BD Biosciences) running FACSDiva software (serial passaging and H-ras expression yielded cultures with approximately 90% and 50% GFP^+ cells, respectively). Sorted cells were transferred to polyethylenimine-coated chambered slides and stained for SA-β-Gal according to manufacturer's instructions (Cell Signaling).

qRT–PCR and flow cytometry. RNA extraction, cDNA synthesis and qRT–PCR from whole-mouse tissue were performed as previously described[15]. To perform qRT–PCR on GFP^+ and GFP^- cell populations of IAT, single-cell suspensions of stromal vascular fraction were prepared from ~50 mg IAT as described[28]. Cell sorting was performed as described above. RNA was extracted from the collected cells using an RNeasy Micro Kit (Qiagen) and cDNA synthesized using a WT-Ovation RNA Amplification kit (NuGEN Technologies), according to the manufacturers' protocols. qRT–PCR primers were as follows: FKBP–Casp8 forward, GAATCACAGACTTTGGACAAAGTT; FKBP–Casp8 reverse, GGTCAAAGC CCCTGCATCCAAG; EGFP forward, CAAACTACAACAGCCACAA CG; EGFP reverse, GGTCACGAACTCCAGCAG. Sequences of other primers used were as previously described[15].

Analysis of progeroid phenotypes. Bi-weekly checks for lordokyphosis and cataracts were performed as described[15]. Skeletal muscle fibre diameter measurements were performed on cross-sections of gastrocnemius and abdominal muscles of female mice as described[15]. Fifty total fibres per sample were measured using a calibrated computer program (Olympus MicroSuite Five). Fat cell diameter measurements were performed on IAT according to the same method. Dissection, histology and measurements of dermal and adipose layers of skin were performed as described previously[12], although the lateral skin between the front and hind limb was used because this adipose layer is nearly three times thicker than dorsal skin. Measurements of body weight, length, gastrocnemius muscle and assorted adipose depots were performed on 10-month-old females. Bone mineral content, bone mineral density and total body adipose tissue were analysed by DEXA scanning as previously described[6]. Exercise measurements were performed on 10-month-old mice as previously described[29]. Animals were acclimated for 3 days for 5 min at a speed of 5 m min^{-1} before experimentation. For the experiment, the speed of the treadmill began at 5 m min^{-1} and was increased to 8 m min^{-1} after 2 min. Thereafter, the speed was increased at a rate of 2 m min^{-1} every 2 min and the time (in seconds) and distance (in metres) to exhaustion, as defined by an inability to move along the treadmill with stimulation, were determined. The formula to determine the amount of work (*J*) performed was: mass (kg) × *g* (9.8 m s^{-2}) × distance (m) × *sin*(θ) (with an incline of θ = 5°). Cardiac arrhythmia measurements were performed using a Vevo2100 ultrasound system (Visualsonics) as previously described[30].

***In vivo* BrdU incorporation and SA-β-Gal staining.** Analyses for *in vivo* BrdU incorporation were performed in 10-month-old female mice as described[15]. Adipose tissue depots were stained for SA-β-Gal activity as previously described[12].

25. Soleimani, M. & Nadri, S. A protocol for isolation and culture of mesenchymal stem cells from mouse bone marrow. *Nature Protocols* **4,** 102–106 (2009).
26. Malureanu, L. *et al.* Cdc20 hypomorphic mice fail to counteract de novo synthesis of cyclin B1 in mitosis. *J. Cell Biol.* **191,** 313–329 (2010).
27. Dimri, G. P. *et al.* A biomarker that identifies senescent human cells in culture and in aging skin *in vivo*. *Proc. Natl Acad. Sci. USA* **92,** 9363–9367 (1995).
28. Kirkland, J. L., Hollenberg, C. H. & Gillon, W. S. Effects of fat depot site on differentiation-dependent gene expression in rat preadipocytes. *Int. J. Obes. Relat. Metab. Disord.* **20** (Suppl 3), S102–S107 (1996).
29. LeBrasseur, N. K. *et al.* Myostatin inhibition enhances the effects of exercise on performance and metabolic outcomes in aged mice. *J. Gerontol. A Biol. Sci. Med. Sci.* **64A,** 940–948 (2009).
30. Martinez-Fernandez, A. *et al.* iPS programmed without c-MYC yield proficient cardiogenesis for functional heart chimerism. *Circ. Res.* **105,** 648–656 (2009).

doi:10.1038/nature10600

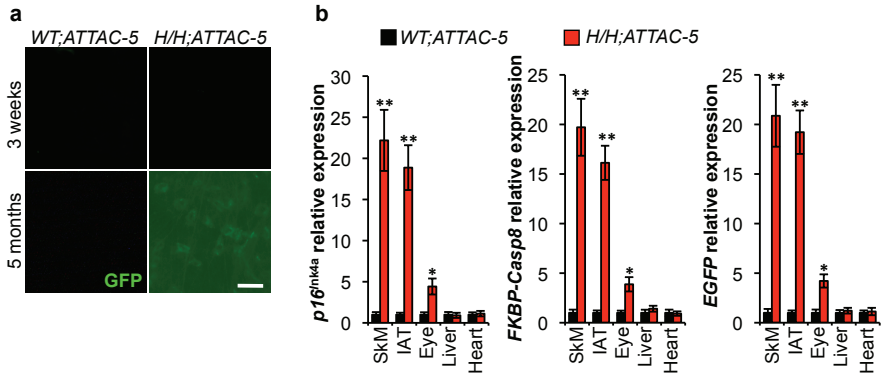

Supplementary Fig. 1: Validation of *p16*^{Ink4a}-specific expression of the *INK-ATTAC-5 transgene.* **a**, GFP intensity of IAT collected from 3-week and 5-month-old untreated mice with the indicated genotypes. Scale bar, 20 μm. **b**, qRT-PCR analysis of untreated 10-month-old mouse tissue analyzed for the relative expression of *p16*^{Ink4a}, *FKBP-Casp8*, and *EGFP*. Error bars, s.d.; *n* = 3 female mice per genotype. **P < 0.05, **P < 0.01*.

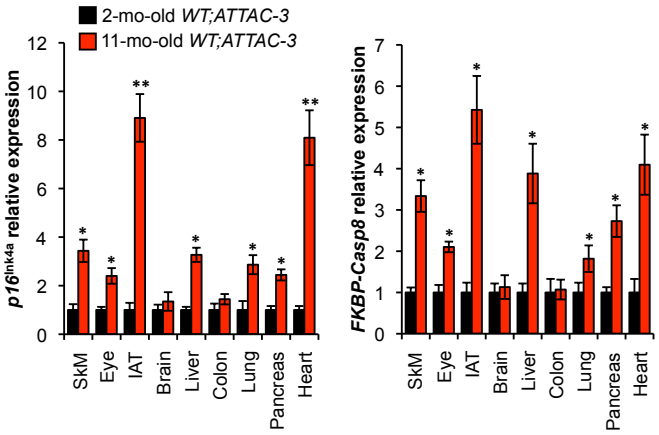

Supplementary Fig. 2: *p16*^{Ink4a} and *INK-ATTAC* expression concurrently increase with chronological aging. Analysis of *p16*^{Ink4a} and *INK-ATTAC* expression in various tissues of 2- and 11-month-old *WT;INK-ATTAC* mice. Error bars, s.d.; *n* = 3 females per age group. **P < 0.05, **P < 0.01.*

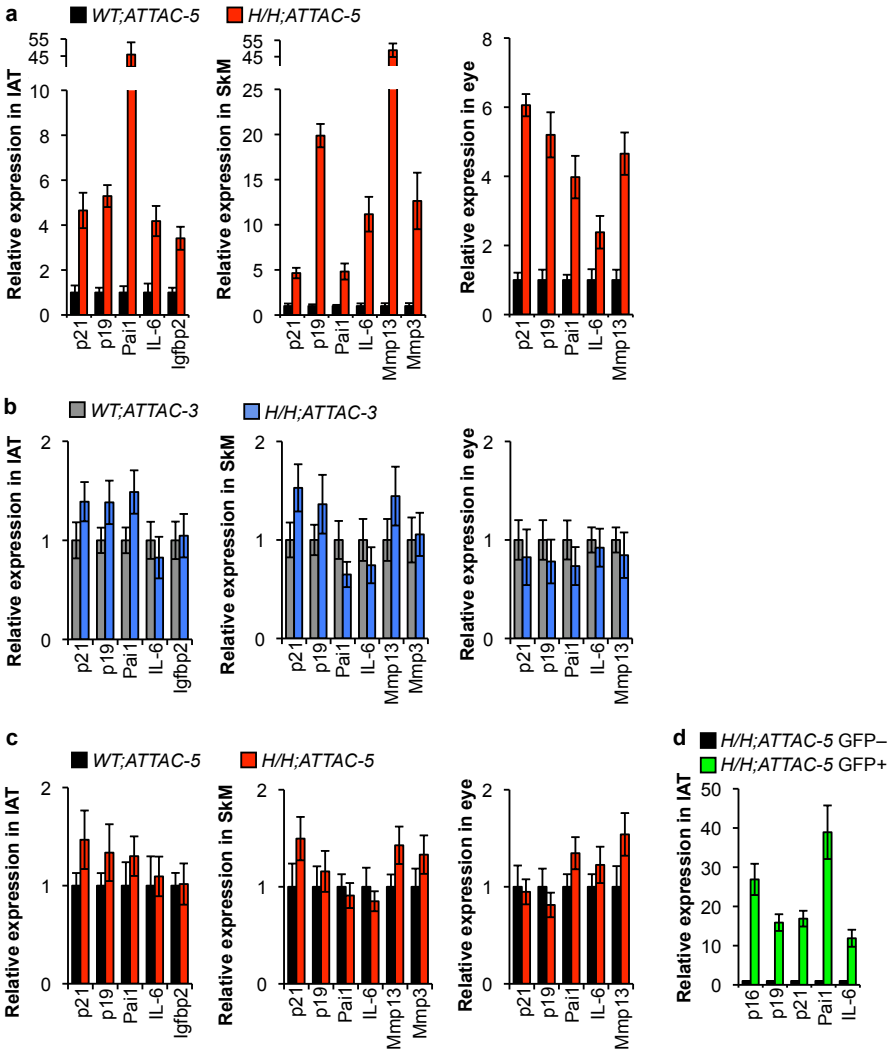

Supplementary Fig. 3: Tissues expressing the *INK-ATTAC-5* transgene display elevated indicators of senescence. **a**, Relative expression of senescence markers in the indicated tissues of 10-month-old *BubR1*$^{H/H}$*;INK-ATTAC-5* and *WT;INK-ATTAC-5* mice as measured by qRT-PCR. All increases are statistically significant ($P < 0.05$). **b**, Relative expression of senescence markers in the indicated tissues of 3-week-old *WT;INK-ATTAC-3* and *BubR1*$^{H/H}$*;INK-ATTAC-3* mice as measured by qRT-PCR. There were no significant differences. **c**, As in **b** but for 3-week-old *WT;INK-ATTAC-5* and *BubR1*$^{H/H}$*;INK-ATTAC-5* mice. **d**, GFP^{+} and GFP^{-} cell populations from IAT of 10-month-old *BubR1*$^{H/H}$*;INK-ATTAC-5* mice analyzed for relative expression of various senescence markers by qRT-PCR. All increases are statistically significant ($P < 0.01$). Error bars, s.d.; n = 3 female mice per genotype

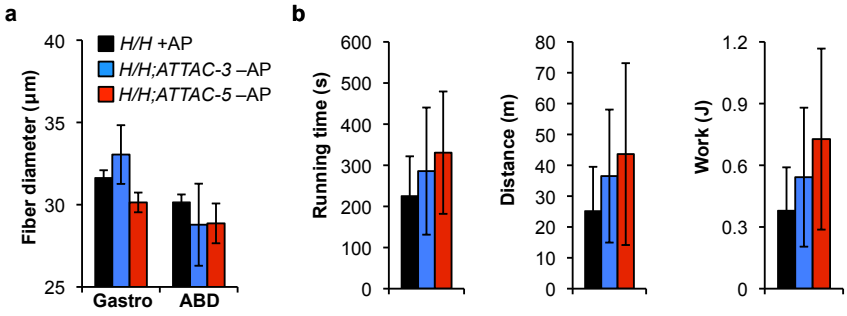

c

Mouse (treatment)	Weight (g)	Fat (%)	POV (g)	Peri (g)	IAT (g)	Mes (g)	SSAT (g)	Brown (g)
H/H (+AP)	18.2 (2.9)	16.1 (1.9)	0.100 (0.04)	0.011 (0.003)	0.068 (0.03)	0.078 (0.01)	0.060 (0.01)	0.095 (0.016)
H/H;ATTAC-3 (–AP)	17.4 (1.8)	15.6 (3.4)	0.054 (0.05)	0.016 (0.02)	0.058 (0.02)	0.063 (0.05)	0.038 (0.01)	0.084 (0.005)
H/H;ATTAC-5 (–AP)	16.7 (2.2)	15.4 (2.5)	0.137 (0.13)	0.020 (0.01)	0.075 (0.05)	0.061 (0.04)	0.050 (0.02)	0.104 (0.030)

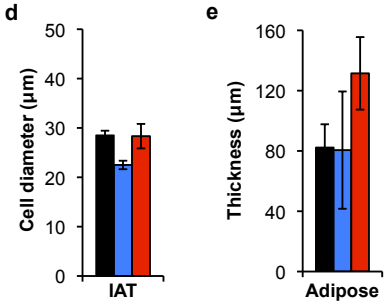

Supplementary Fig. 4: AP20187 treatment of *BubR1*$^{H/H}$ mice does not delay *p16*^{Ink4a}-mediated age-related phenotypes in the absence of *INK-ATTAC*. **a**, Mean muscle fiber diameters of gastrocnemius and abdominal muscles of 10-month-old AP20187-treated *BubR1*$^{H/H}$ mice and non-treated *BubR1*$^{H/H}$;*INK-ATTAC* mice. **b**, Exercise ability of 10-month-old AP20187-treated *BubR1*$^{H/H}$ mice and non-treated *BubR1*$^{H/H}$;*INK-ATTAC* mice. **c**, Body and fat depot weights of 10-month-old AP20187-treated *BubR1*$^{H/H}$ mice and non-treated *BubR1*$^{H/H}$;*INK-ATTAC* mice. Parentheses, s.d. **d**, Mean fat cell diameters in IAT of 10-month-old AP20187-treated *BubR1*$^{H/H}$ and untreated *BubR1*$^{H/H}$;*INK-ATTAC* mice. **e**, Subcutaneous adipose layer thickness of 10-month-old AP20187-treated and untreated *BubR1*$^{H/H}$;*INK-ATTAC* mice. Color codes in **b**, **d** and **e** are as indicated in **a**. Error bars indicate s.e.m. in **a**, **d** and **e**, and s.d. in **b**. For all analyses n = 6 female mice per genotype.

a

Genotype (treatment)	BPM (SD)	Sinus pauses % (SD)
WT;ATTAC-3 (–AP) n=3	485.3 (24.7)	0.024 (0.005)
H/H;ATTAC-3 (–AP) n=6	482.5 (35.2)	2.237 (0.135)
H/H;ATTAC-3 (+AP) n=6	456.7 (38.3)	2.176 (0.161)
WT;ATTAC-5 (–AP) n=3	480.8 (29.3)	0.021 (0.004)
H/H;ATTAC-5 (–AP) n=6	466.7 (31.3)	2.124 (0.221)
H/H;ATTAC-5 (+AP) n=6	475.2 (33.9)	2.046 (0.169)

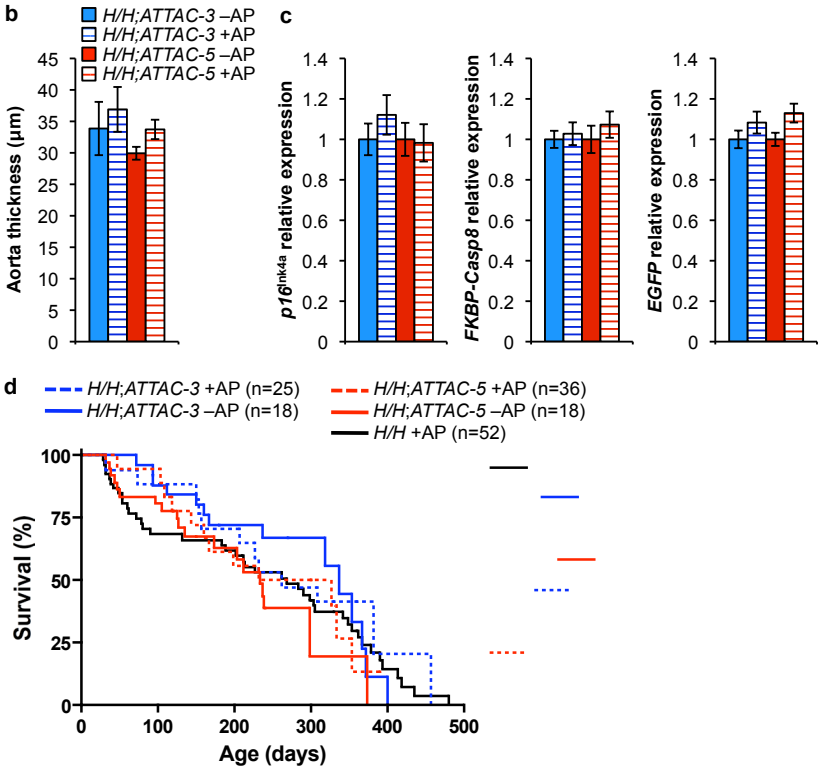

Supplementary Fig. 5: Age-associated traits of BubR1 hypomorphic mice that are *p16*^{Ink4a}-independent are not influenced by clearance of *p16*^{Ink4a}-positive cells. a, Measurement of heart sinus pause rhythm disturbances in mice of the indicated genotypes and treatments. Abbreviation: BPM, beats per min. **b**, Thinning of the aorta is not corrected by drug treatment in *BubR1*$^{H/H}$*;INK-ATTAC* animals. Error bars, s.e.m.; *n* = 6 female mice per genotype. **c**, qRT-PCR analysis of *p16*^{Ink4a} and *INK-ATTAC* expression in aortas of the indicated mice. Error bars, s.d.; *n* = 3 female mice per genotype per treatment. **d**, Survival curves of AP20187-treated and untreated *BubR1*$^{H/H}$*;INK-ATTAC* and AP-treated *BubR1*$^{H/H}$ mice. We note that cardiac stress tests performed on *BubR1*$^{H/H}$ mice indicate that cardiac failure is likely to be the primary cause of death of these animals.

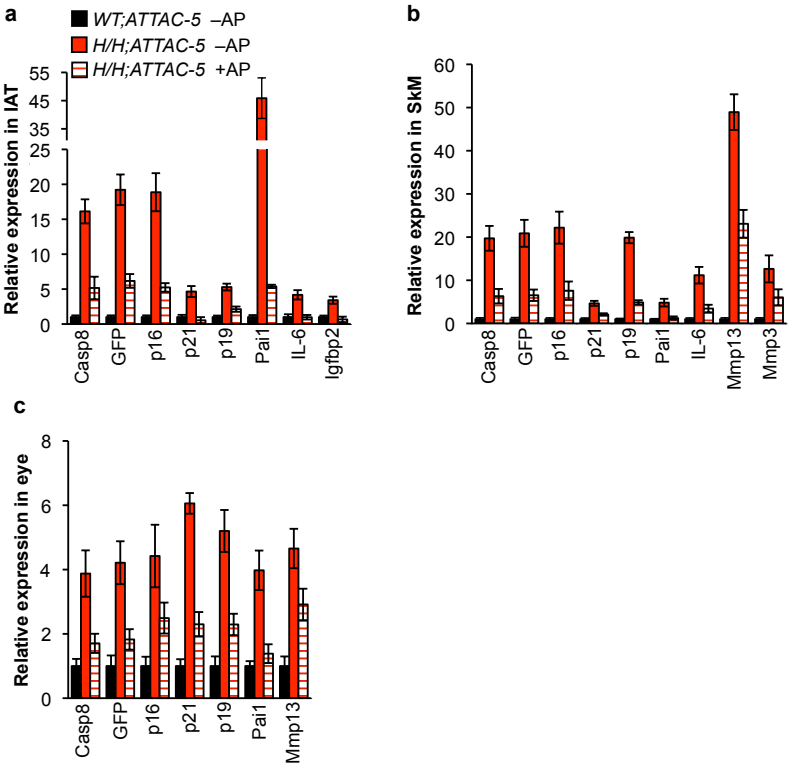

Supplementary Fig. 6: AP20187 treatment of *BubR1*$^{H/H}$*;INK-ATTAC-5* animals reduces p16^{Ink4a}-positive senescent cells. qRT-PCR analysis for indicators of senescence in IAT (**a**), skeletal muscle (gastrocnemius), (**b**) and eye (**c**) reveals that treatment of animals with AP20187 leads to lower levels of senescence-associated markers. Error bars, s.d.; n = 3 female mice per genotype. All genes have a significant decrease upon AP20187 treatment ($P < 0.05$).

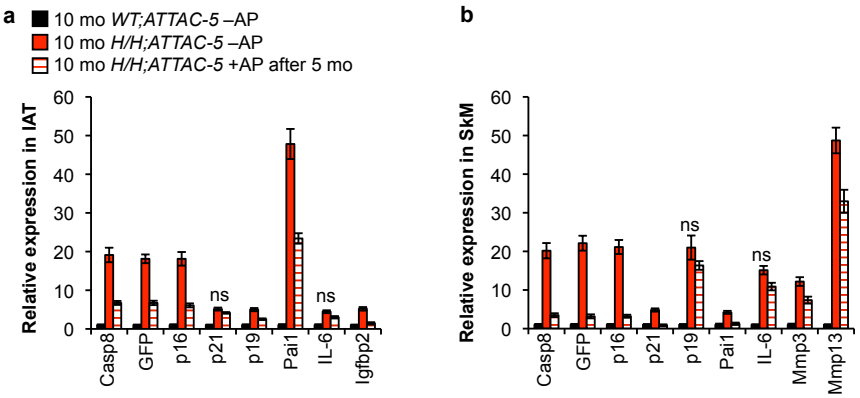

Supplementary Fig. 7: Late-life treatment of *BubR1*$^{H/H}$*;INK-ATTAC-5 animals reduces p16*^{Ink4a}*-positive senescent cells. qRT-PCR analysis for indicators of senescence in IAT (**a**) and skeletal muscle (gastrocnemius) (**b**) reveals that treatment of animals with AP20187 leads to lower levels of senescence-associated markers. Error bars, s.d.; *n* = 3 female mice per genotype. All genes (except those marked with ns) have a significant decrease upon AP20187 treatment (*P < 0.05*).